Silo: Half-Gigapixel Cylindrical Stereoscopic Immersive Display

Category: System

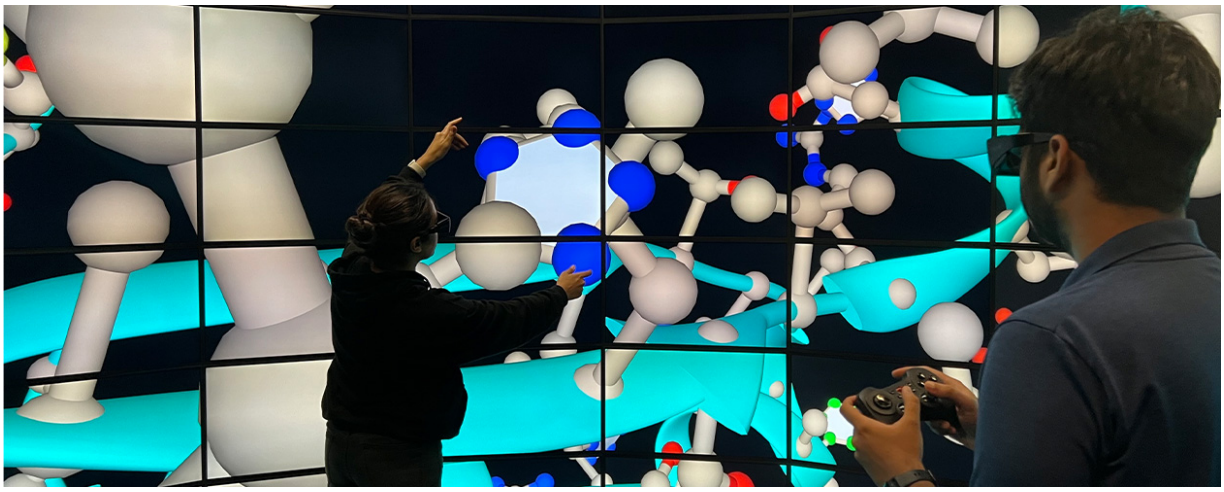

Figure 1: Two scientists studying the 3D structure of a protein in the Silo – a high-resolution immersive stereo visualization facility.

ABSTRACT

We present the design and construction of the Silo, a fully immersive stereoscopic cylindrical tiled-display visualization facility. Comprising 168 high-density LCD displays, the facility provides 619 million pixels, and close to 360 horizontal field-of-regards (FoR), aiming to maximize visual acuity and completely engage the human visual sensorium and its periphery. In this article, we outline the motivations, design principles, hardware selection and software systems, and interaction modalities used in constructing the Silo. To address missing visual information due to the absence of a ceiling and floor, we have designed a method that utilizes conformal mapping and optimal mass transport to reproject the entire 360 volumetric FoR of the virtual scene to the available screen real estate. We showcase several applications demonstrating the utility of the Silo and report the findings of our user studies that highlight the effectiveness of the Silo layout compared to curved mono and flat powerwall display facilities. Our user evaluations and studies have shown that the Silo supports natural exploration and enhanced visualization due to its capability to render surround high-resolution stereoscopic views.

Index Terms: Immersive Visualization, High-resolution Display, Data Visualization, CAVE, Conformal Visualization

1 INTRODUCTION

The advancement in display and GPU technology over the past decades has pushed the frontiers of immersive visualization (IV). Systems for IV have propelled novel methods for scientific investigation and data exploration through their capability to "put users within their data". Unlike traditional desktop settings, which aim to provide visualizations within the constraints of a single screen, IV platforms deliver a greater volume of information to the user by significantly widening the available field-of-view (FoV) and field-of-regard (FoR). As such, it has been shown that for vast 3D data, such as molecular structures, geoscience information, engineering models, and biomedical volumes, IV environments not only enhance the perception of depth and spatial relationships within complex datasets but also improve performance when carrying out analytical tasks [25].

Towards this goal, the visualization and human-computer interaction communities have since long made significant contributions: from the pioneering CAVE technology [10] to its new-generation shape and configuration variants – large high-resolution display walls (or sometimes referred to as power-walls), room-sized gigapixel facilities [33], and in more recent times, commodity head-mounted displays (HMDs). Each modality has demonstrated its unique utility in data visualization, interaction, and exploration.

Broadly, the design of an IV system is driven by two factors: visual acuity and degree of immersion. Visual acuity is the quality of the visuals a display can deliver, whereas the degree of immersion is the suspension of disbelief that a visualization system provides. However, these attributes can present a dichotomy. High-resolution and large screen real-estate are key resources for improving the visual acuity for large-scale and complex datasets, making power-walls more appropriate, albeit lacking immersion. Conversely, HMDs and CAVE systems can significantly enhance a user's sense of immersion. However, the current state-of-the-art hardware in HMD lenses, projectors, or LCD panels has limited pixel density.

Motivated by this situation, the lessons learned, and the vision for the future of IV systems [12], we have designed and built the Silo, an immersive visualization facility that maximizes both visual acuity and immersion. It comprises high-pixel-density displays, connected to an active stereo system, and arranged in a 4.8m diameter wide $\times$ 2.4m tall cylindrical configuration, offering 619 million pixels on a continuous surface with 20/20 visual acuity and 330-degree horizontal FoR. This configuration allows multiple users to intuitively examine data at various scales by approaching or distancing themselves from the displays while preserving rotational navigation and the panoramic context of the data. To the best of our knowledge, the Silo is the highest-resolution stereo display facility at this scale. Fig. 1 shows a close-up picture of users collaborating in the Silo and Fig. 2 shows a 3D rendering of the Silo facility, along with some of its hardware configurations.

The construction of immersive facilities using panel displays is often challenged by the absence of at least one display surface, such as the ceiling, floor, or entrance, adversely affecting information coverage and general navigation capabilities. To solve for miss-

ing display surfaces, Petkov et al. [38] have developed a conformal mapping approach that transforms scene geometries from a fully enclosed planar 6-sided CAVE, with a *cubical* layout, to any partial display configuration. Mathematically, a conformal map is an angle-preserving function that describes a mapping between two Riemannian surfaces such that the transformation preserves local shapes [43]. However, when applied to a cylindrical facility, this method allocates disproportionate area ratios: the recovered ceiling and floor cover more of the scene in the Silo than the central cylinder region. To address this, we further optimize the final scene map by employing area-preserving optimal transformation mapping on the conformal map. An optimal transportation map transports a probability measure to another probability measure in the most economical way [44]. Specifically, we calculate a composition of angle-preserving conformal and area-preserving optimal transport mapping to transforms the viewing directions from a closed capsule configuration (cylindrical middle section with two hemispherical ends) to the open-cylindrical Silo.

Finally, we demonstrate the utility of the Silo through user studies focused on tasks requiring depth perception, object identification, and navigation in complex 3D environments, comparing user experience and performance across stereo and mono displays, as well as against a planar mono powerwall. The study reveals that the Silo consistently outperforms other settings in terms of efficiency, task success rates, and workload reduction, as indicated by quantitative metrics (task completion times, success rates, NASA-TLX assessments) and qualitative user feedback.

2 Related Works

Immersive visualization environments have significantly evolved over the years, offering increasingly sophisticated solutions to visualize complex data. One of the earliest systems in this domain is the CAVE (Cave Automatic Virtual Environment) [27], developed by the Electronic Visualization Laboratory (EVL). The CAVE, with its cube-shaped design, provides a fully immersive experience where users can interact with 3D visualizations projected onto the walls, ceiling, and floor. This pioneering system laid the groundwork for many subsequent developments in IV facilities.

Subsequently, the Cornea [11], a six-sided facility at King Abdullah University of Science and Technology, and AixCAVE [24], a five-sided facility at RWTH Aachen University have been constructed with enhanced high-resolution stereoscopic projection. Beyond the original CAVE design, StarCAVE [13] took a different approach with its five-sided pentagonal structure, providing a 360°view with stereoscopic projection. It is particularly effective for geospatial data visualization, allowing users to explore large-scale landscapes and urban environments. AlloSphere at the University of California[22] also diverges from the traditional CAVE by offering a three-story spherical immersive environment. It additionally employs spatialized sound, creating a multi-sensory experience. This environment is particularly advantageous for exploring complex scientific phenomena, engaging both visual and auditory senses for more profound insight.

The advancements in LCD technology in the early 2000s resulted in the emergence of tiled-display facilities as a more feasible solution for large-scale visualization. These facilities, often covering expansive areas, deliver high image quality and resolution with minimal upkeep. They allow for the detailed visualization of large datasets while maintaining context, paving the way for new opportunities in collaborative data analysis. CAVE2 [16], the next-generation CAVE at EVL, utilized LCD technology and constructed a hybrid reality environment composing 72 displays in a cylindrical configuration. It supports 2D and 3D data visualization and is designed for collaborative research, allowing multiple users to engage with the data simultaneously.

The Reality Deck [33] at Stony Brook University pushed the resolution boundaries by combining 416 displays to offer 1.6 billion pixels. This 4-walled, room-sized facility significantly enhances the sense of immersion and enables 20/20 visual acuity. Applications in the Reality Deck can handle extensive data sizes, making it ideal for with natural focus+context visual analysis of large data, such as geoscience, astronomy, and biomedical visualization. In contrast, DSCVR [39] focused instead on a smaller number of high-resolution displays, attempting to tackle concerns surrounding the scalability, reconfigurability, and accesibilty of IV environments. As such, it demonstrates the utilization of commodity-grade hardware to create a cost-effective hybrid reality environment.

In re-imagining IV facilities, DataSpace [9] focused its design as a collaborative immersive environment by offering a reconfigurable hybrid reality space. The setup comprises moveable high-resolution displays, augmented reality headsets, and a central interactive table. It differentiates itself from its predecessors with a design aimed at spatial reconfigurability, scalability, and equitable access to data, envisioning modern hybrid immersive environments.

Together, these systems illustrate the extensive and ongoing innovation in immersive visualization technologies. They encompass a range of designs, from the original cube-shaped CAVEs to spherical and cylindrical configurations, each uniquely tailored for specific research applications. Silo, builds on these developments by integrating high-resolution visualization, immersion, and navigation within its cylindrical environment. This facility is arguably the highest-resolution, high pixel-denisty, stereoscopic IV facility.

3 Silo

The choice of hardware in constructing the Silo and the configuration of its layout was guided by key design principles outlined in the literature for designing IV facilities:

- **D1** A large, high-resolution display facility that approaches the sphere of influence and perception of a human [2].
- **D2** A physical space that can accommodate multiple users for supporting co-located collaboration.
- **D3** In choosing display hardware, it should strike the right resolution target such that the pixel density reaches the visual acuity of the human visual system [16, 33].
- **D4** Support for stereoscopic rendering.

Large, high-resolution displays are a valuable instrument for exploring large amounts of information [32]. Belkasim et al. [6] defined these facilities as "a coherent physical view space that is at least of the size of the human body and exhibits a significantly higher resolution than a conventional display." In contrast to modern commodity HMD technology, they enable physical navigation of the virtual content rather than moving a virtual camera within a 2D or 3D coordinate system. In a way, physical navigation enables the use of different cognitive resources, which consequently enhances spatial memory [40] and the use of peripheral vision for certain tasks [4, 23]. Regarding display form-factor, curved arrangements have been shown to be effective for IV systems [5, 26]. Compared to a traditional flat or planar layout, such as powerwalls or 4- to 6-sided CAVEs, the Silo surrounds the human FoR with the virtual environment along the horopter, thus enhancing the degree of immersion and mitigating out-of-sight data due to extreme angles. Moreover, when designing a shared physical space for multi-user collaboration, a circular arrangement allows for rotational navigation, which is a natural form of visual exploration that is less physically demanding than walking to change one's viewpoint.

Based on these factors, we have constructed the Silo as an *open* icositrigon (23-gon) structure to imitate an open cylindrical IV facility (**D1, D2**). Specifically, 21 planar display columns are arranged in a circular configuration, with an opening serving as an entrance. The facility has no displays on the ceiling and floor.

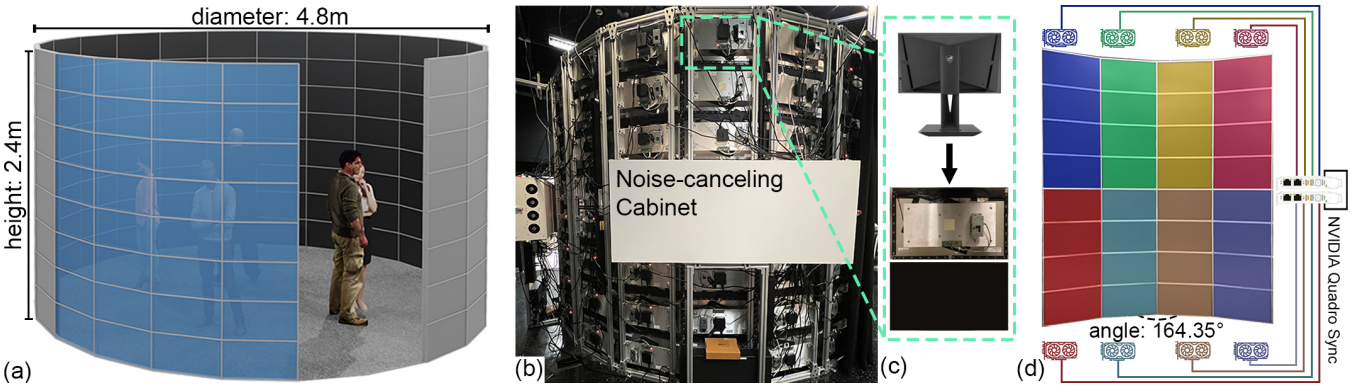

Figure 2: (a) 3D rendering of the Silo model. (b) The back-side of one Silo node, showing our custom-designed aluminium mount frame and the noise canceling cabinet for the machine. (c) An inset showing our display customization from the manufacturer product, to reduce bezel size. (d) A diagram illustrating the GPU configuration in each node.

Fig. 2 (a) depicts a synthetic, to-scale rendering of the facility. This layout provides an open space of 16 feet in diameter for multiple users, comfortably fitting 6-7 people for collaboration.

Papadopoulos et al. [32] have published an elaborate user study that quantifies the performance implications of large, physically-navigated, high-resolution displays for four display resolutions: 100 megapixels, 300 megapixels, 600 megapixels, and one gigapixel. Their findings showed that normalized user performance plateaued past the 600 megapixel point. Based on this study and to support **D3**, we have designed the Silo to consist of 162 QHD display monitors, each with resolution 2560×1440, totaling 619.32 megapixels. Furthermore, it has been shown that using stereoscopic technologies in virtual environments allows the users to perceive depth with greater accuracy, enhances their immersive experience and interpretation of 3D models, and increases productivity [8, 31]. As a result, to maintain a high pixel resolution and density for stereo rendering (**D4**), we chose displays with high refresh rates that can support an active stereo system.

4 Hardware and Configuration

When building a large-scale IV facility, each component, from the display system to the visualization cluster, influences its overall performance and user experience. This section outlines several hardware and software engineering and design decisions we made during the construction of the Silo.

4.1 Display Selection and Layout

Arguably, the most critical component of any visualization environment is its display. Large IV systems have evolved from using projectors to high-resolution LCD displays. In addition to the design goals, our choice for the Silo display hardware was influenced based on the following criteria outlined in the literature [33, 16, 11]:

- *Image quality*: The display panels should be high-quality with good contrast, backlight uniformity, and large viewing angles.
- *Resolution target*. To achieve a high-resolution target, the monitors should provide ∼100 pixels per inch (PPI).
- *Bezel size*. Ideally, the bezel should be as narrow as possible; however, it should not exceed 8mm for a 23in. display and 15mm for a 30in. display.
- *Stereo support*. Stereo is very desirable, but not at the cost of significantly reduced pixel density.

We evaluated several commercially available displays with varying panel and bezel sizes and technologies. To best achieve the design goals and display criteria, we eliminated projector technology due to its low-resolution target and image quality. Moreover, we could not proceed with micrometer LED and OLED panels due to their high initial and maintenance costs (given the required PPI and laser alignment to maintain the proposed facility dimensions). Amongst LCD technology, the challenging factors were balancing bezel size and stereo support.

Several research groups and facilities have achieved high-resolution mono IV systems. Thus, we were motivated to construct a facility that breaks the barrier for a high-resolution and high-pixel-density stereo visualization system. Balancing all factors, we opted for commercially available ASUS ROG SWIFT PG278QR panels [3], a professional 27-inch QHD twisted nematic (TN) panel with 2560×1440 resolution with excellent contrast and color saturation. TN panels are the fastest (with minimal motion blur and low input lag) and cheapest panel technology, hence their prevalence in gaming monitors and laptops, albeit at the cost of lower viewing angles. This was important to us because a high refresh rate of 165Hz allowed us to employ an active stereo system without compromising pixel resolution. The low 170° horizontal viewing angle did not cause an issue since each display column is rotated to form the circular configuration (details mentioned below). Finally, although the original bezel is 6mm, we modified the monitors with a custom mount that reduced the bezel to 4mm, as shown in the inset in Fig. 2 (c).

Given the available physical space, design goal **D1**, and to achieve an optimal 600 megapixels resolution [32], we arranged the displays in the following configuration: 21 display columns, with each column 8feet (2.4384m) high, rotated 15.652° from the center of the facility with radius 8feet (2.4384m), and each column comprising 8 display panels (in landscape orientation). As a result, the Silo consists of 168 display panels. To mount the displays, we designed custom mounting brackets and an aluminum frame so that individual monitors can be aligned with sub-millimeter accuracy (confirmed via laser leveling). Fig. 2 (b) shows our custom-designed aluminum frame with the monitors mounted on them.

4.2 Visualization Cluster and Configuration

The visualization cluster driving the Silo consists of six nodes. Five nodes power 32 display panels (4 columns) each and are equipped with the following:

- 2×Intel Xeon Silver 4210R Processor(10 Core, 2.40Ghz)
- 8×NVIDIA RTX A6000 (48 GB GDDR6)
- 2×NVIDIA Quadro Sync II Board
- 12×16GB DDR4 RAM

The sixth node powers the remainder column with 16 displays, using 2 GPUs and a single Sync board.

Four displays are connected to one GPU, and four GPUs are connected to one NVIDIA Quadro Sync board. A schematic layout of

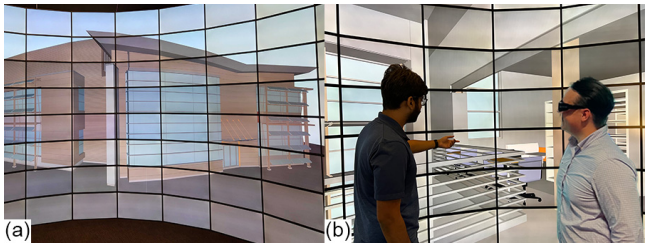

Figure 3: (a) 3D architectural model rendered in the Silo. (b) Architects consulting while visualizing the building 1-1 scale model.

Figure 4: Emergency managers studying flooding scenarios for planning evacuation measures.

the configuration is illustrated in Fig. 2 (d). The Sync board facilitates a highly synchronized and scalable system, aligning display refresh rates across multiple systems and mitigating imaging artifacts in multi-display configurations. Additionally, it supports desktop scalability at the operating system level through NVIDIA Mosaic technology. NVIDIA Mosaic integrates multiple displays into a single cohesive desktop and compensates for physical gaps, such as bezels, between the displays. In our configuration, constrained by the graphics driver resolution limits, we have combined the four displays connected to a GPU into a unified desktop.

For setting up an active stereo system, the Sync boards are daisy-chained, and one node is designated as the timing server. A Volfoni ActiveHub RF emitter [46] is connected to the timing server to synchronize the GPU framebuffer swaps for left- and right-eye with its eye-wears, the Volfoni Edge RF glasses. Thus, in contrast to newer generation passive stereo CAVE systems, the Silo provides full stereo resolution to the user with a high framerate of 60Hz per eye. One hardware limitation deserves to be mentioned here. Prior works in constructing large IV facilities [33] have suggested using fiber-optic display cables with extenders when the cluster nodes are housed at a distance from the displays, such as in a dedicated server room. However, our initial experience exhibited that fiber-optic cables were not resilient for a high-framerate stereo system: often, the graphic card driver would not receive coherent signals, causing the Mosaic configuration to be disturbed or some displays to go out of sync. Subsequently, we reverted to using traditional copper cables. We placed each node next to its display cluster to avoid signal loss or delay due to the extended cable length. Moreover, we designed a custom noise-canceling cabinet for each node (labeled on Fig. 2 (c)) to mitigate machine noise for a better user experience.

5 Applications

Software Architecture To develop applications for the Silo, we have implemented an OpenGL-based framework, which we refer to as the *SiloEngine*. It follows a replicated execution model [14]. That is, instances of a target application are launched individually in the Silo nodes, and a master instance synchronizes components such as application controls, tracking, and communications across all instances and nodes. Specifically, SiloEngine is provided with a configuration file that describes the physical layout of the Silo displays, its initial position in the virtual scene, and the camera viewport for each application instance. Additionally, for each instance, its respective system information, such as the machine name and allocated GPU, is also provided. Assigning a GPU to an instance ensures that the OpenGL context uses the particular GPU for rendering and processing. We have dedicated a separate node primarily for the head instance, with the same computing power. This frees the visualization nodes from the overhead of processing and managing the application synchronization.

Currently, the Silo is equipped with a gamepad controller and OptiTrack infra-red (IR) cameras to support interaction. The interaction data is sent to the master instance's input management using the virtual-reality peripheral network (VRPN) protocol. The master subsequently communicates the interaction input, such as updating the position and orientation of the Silo or any virtual object in the virtual scene, or any processed action to the instances. To maintain scene coherence, the master periodically broadcasts information to the instances, which updates it if out-of-sync.

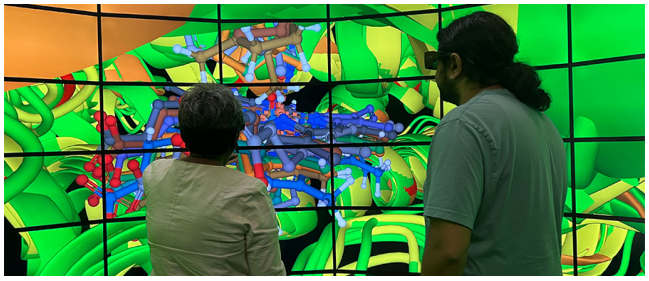

Figure 5: Virologists studying a complex enzyme structure captured using electron microscopy.

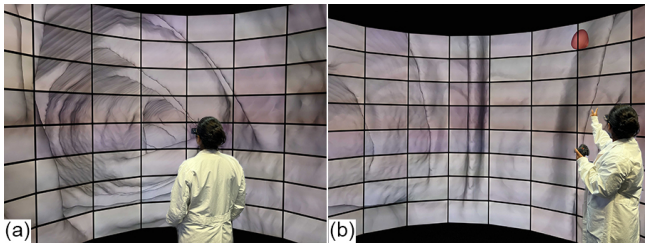

Figure 6: (a) A medical doctor performing colonoscopy in the Silo. (b) The FoR allows the doctor to identify a polyp, hidden behind a fold, with the turn of her head while navigting through the colon.

Applications We now present some applications that demonstrate the utility of the Silo. In this manuscript, all figures showing applications in the Silo are in monoscopic view for picture-quality purposes – that is, to avoid stereo ghosting. Fig. 13 (a), however, has the application in stereoscopic mode. Our supplementary video also shows the applications in stereoscopic mode.

Incorporating VR technologies has been identified as an integral component towards the next revolution in architecture, engineering, and construction [41]. It aids teams in visualizing 3D models of the buildings in a real-scale environment before construction and analyzing various scenarios, such as lighting conditions and changes made to interior designs [1]. Fig. 3 shows such an application developed for the immersive visualization of architectural models in the Silo. We invited stakeholders such as architects, interior designers, and the institution leadership to visualize and study the 3D model of a new building to be constructed on campus. In contrast to traditional desktop settings, the participants shared two essential benefits of studying the model in the Silo. First, the real-scale stereo model enabled an accurate sense of the interior furnishing placements in terms of space and safety precautions. As such, after observing movement spaces, the interior designers made necessary adjustments to furniture in the foyer and laboratory. In another instance, the architects identified a critical change in the safety features of a scaffolding structure on the exterior of the building, which is used for maintenance purposes. Second, the high-resolution fa-

cility enabled the stakeholders to observe and consult texture options for the furnishings and walls holistically at different scales by naturally walking closer to the displays for finer and panoramic observations, respectively.

The increase in extreme weather events has led to a growing need for visualization systems that aid scientists and emergency managers in effectively preparing for impacts and resiliency. We implemented a stereo and cylindrical-layout version of the immersive flooding visualization application, Submerse [7]. As shown in Fig. 4, we invited firefighters and emergency managers to the Silo to collaboratively plan an evacuation procedure based on a simulated flooding scenario. In contrast to a mono-immersive environment, the participants conveyed that the Silo stereo environment provided better depth perception when analyzing factors such as flooding height and landmark distances.

With the advancement in imaging technology, biomedical datasets are growing ever larger and more complex. We have implemented an application that assists scientists in visualizing results from structural bioinformatics (Fig.5) and computer-aided drug design efforts (Fig. 1). Moreover, in the medical domain, we demonstrate the application of immersive virtual colonoscopy (VC) [29], shown in Fig. 6 (a). The stereo and full FoR facilitates enhanced visual exploration as in the case of VC, medical experts are able to identify polyps that could be otherwise occluded due to muscular folds, shown in Fig. 6 (b).

A video exhibiting our applications is included as part of the Supplementary Materials.

6 Visualizing Missing Information

To visualize the information missing due to absent ceiling and floor, we introduce a novel approach that utilizes conformal mapping [37, 28, 47] and optimal transport (OT) mapping [48, 30] techniques. Specifically, we assume a hypothetical Silo with a capsule shape and map the surface from the capsule onto the original Silo surface.

6.1 Conformal Mapping

A conformal mapping between two surfaces with Riemannian metrics $(S_k, \mathbf{g}_k)$, $k = 1,2$, preserves angles and local shapes but distorts areas. Such a mapping $\varphi : S_1 \to S_2$ is defined as conformal if there exists a scalar function $u : S_1 \to \mathbb{R}$, called the *conformal factor*, making the pull-back metric $\varphi^* \mathbf{g}_2$ differ from $\mathbf{g}_1$ by e^{2u}, i.e., $\varphi^* \mathbf{g}_2 = e^{2u(p)} \mathbf{g}_1(p)$ for all $p \in S_1$. This factor quantifies area distortion, and since conformal mappings scale locally, they convert infinitesimal circles while preserving the angles between curves. We utilize these mappings to project the capsule surface onto the Silo for visualization. The conformal mapping can be calculated using the surface *Ricci curvature flow* method [21]

$$\frac{d\mathbf{g}(p,t)}{dt} = 2(\bar{K}(p) - K(p,t))\mathbf{g}(p,t),$$

where $K, \bar{K}$ are the current and the target Gaussian curvature at the point p. Ricci flow, crucial to Perelman's proof of the Poincaré conjecture [34, 36, 35], effectively adjusts Riemannian metrics to achieve specific Gaussian curvatures. This approach has been adapted to discrete surfaces, with solid theoretical backing for the existence and uniqueness of solutions in discrete settings [18, 17].

A discrete setting can be defined as a surface S with a triangulation $\mathscr{T}$ and a polyhedral metric $\mathbf{g}$, such that vertices $V(\mathscr{T})$ are cone singularities, and everywhere else if flat (Gaussian curvature is zero). The polyhedral metric $\mathbf{g}$ is represented by the edge length function: $l : E(\mathscr{T}) \to \mathbb{R}_{>0}$, such that on each face $f \in F(\mathscr{T})$ the triangle inequality holds, and f is treated as a Euclidean triangle. Suppose a face f_{ijk} with three vertices $\{v_i, v_j, v_k\}$, the edge lengths against them are l_i, l_j, l_k, then the *cosine law* is

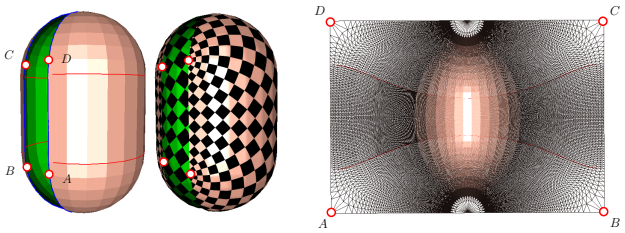

Figure 7: Conformal mapping using Ricci flow, all the right angles of the checkers are well preserved.

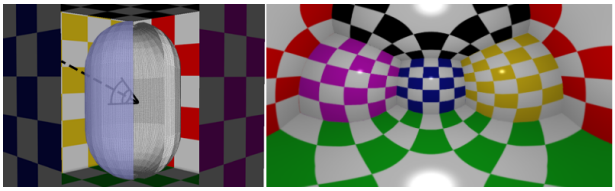

Figure 8: Conformal texture generation by ray tracing.

$\cos\theta_i^{jk} = (l_j^2 + l_k^2 - l_i^2)/(2l_j l_k)$. The *discrete Gaussian curvature* at the vertex $v_i \in V(\mathscr{T})$ is defined as the angle deficit,

$$K(v_i) = \begin{cases} 2\pi - \sum_{f_{ijk}} \theta_i^{jk} & v_i \notin \partial S \\ \pi - \sum_{f_{ijk}} \theta_i^{jk} & v_i \in \partial S \end{cases} \tag{1}$$

The total Gaussian curvature satisfies the *Gauss-Bonnet* theorem,

$$\sum_{v_i \in \partial S} K(v_i) + \sum_{v_j \notin \partial S} K(v_j) = 2\pi\chi(S), \tag{2}$$

where $\chi(S)$ is the Euler characteristic number of the surface. The *discrete conformal factor* is defined on vertices $u : V(\mathscr{T} \to \mathbb{R}$, and the conformal deformation is discretized as follows: for edge e_{ij} with vertices v_i, v_j, $l_{ij} = \exp(u_i + u_j)\beta_{ij}$ where β_{ij} is the initial edge length of e_{ij}. The *discrete surface Ricci flow* is defined as

$$\frac{du(v_i)}{dt} = 2(\bar{K}(v_i) - K(v_i)), \tag{3}$$

which is the gradient flow of the *discrete entropy energy*:

$$E(\mathbf{u}) := \sum_{v_i \in V(\mathscr{T})} \bar{K}(v_i)u(v_i) - \int_{\mathbf{0}}^{\mathbf{u}} \sum_{v_i \in V(\mathscr{T})} K(v_i)du(v_i). \tag{4}$$

with the gradeint $\nabla E(\mathbf{u}) = (\bar{K}(v_i) - K(v_i))$, and the Hessian:

$$\frac{\partial^2 E(\mathbf{u})}{\partial u_i \partial u_j} = -\frac{\partial K_i(\mathbf{u})}{\partial u_j} = \begin{cases} w_{ij} & i \neq j, \\ -\sum_k w_{ik} & i = j. \end{cases} \tag{5}$$

where w_{ij} is the *cotangent edge weight* [20]. A triangulation $\mathscr{T}$ is called *Delaunay* if for each interior edge e_{ij}, its cotangent wedge w_{ij} is non-negative. The entropy energy is concave and has a unique global maximum [18, 17], the discrete metric at the optimum gives the target curvature. The energy can be optimized using Newton's method. During optimization, the triangulation is updated to Delaunay by edge swappings.

As illustrated in Fig. 7, the corner vertices of the capsule surface boundary are identified as A, B, C, D and set with target curvatures of $\frac{\pi}{2}$, while other vertices have target curvatures of 0. Utilizing discrete Ricci flow, the target metric is achieved, allowing the capsule's triangle mesh to be isometrically flattened into a planar rectangle as depicted in the right frame. The checkerboard texture mappings illustrate that while the checkerboard's right angles remain intact, the sizes of the checkers exhibit distortion.

To generate an environment map, we place the capsule inside a cube map, with a camera at the center of the capsule. For each point p on the capsule surface S, we issue a ray starting from the camera through p and use conventional ray tracing to determine the ray color (Fig. 8). This mapping from S to the color space is defined as $\psi : S \to \mathscr{C}$, where $\mathscr{C}$ is the color space. By composition $\psi \circ \varphi^{-1}$, where φ is the conformal mapping from the S to the Silo surface.

6.2 Optimal Transportation Map

It can be observed in Fig. 8 that the right angles on the checkerboard are well preserved; however, the areas of the black ceiling and the green floor are larger compared to the center. This is because conformal mapping preserves angles but distorts areas. To solve this, we additionally apply OT mapping, which, in contrast, preserves areas but distorts angles.

We implement OT area-preserving maps based on [47, 48, 42]. An OT map transports probability measures in the most economical way [44, 45]. Suppose that the planar source domain with a source measure is (Ω, μ), the target planar domain with a measure is (Ω^*, ν), the total source measure is equal to the total target measure $\mu(\Omega) = \nu(\Omega^*)$. A mapping $T : \Omega \to \Omega^*$ is *measure preserving*, denoted as $T_\# \mu = \nu$, if for any boreal set $B \subset \Omega^*$, $\mu(T^{-1}(B)) = \nu(B)$. Given a *cost function* $c : \Omega \times \Omega^* \to \mathbb{R}_{\geq 0}$, the *optimal transport map* is defined as

$$\min_{T_\# \mu = \nu} \int_\Omega c(x, T(x)) d\mu(x).$$

If the target domain Ω^* is convex, the cost function is the L^2 distance $c(x,y) = |x-y|^2/2$, then the Brenier's theorem [44] claims that there is a convex Brenier potential $u : \Omega \to \mathbb{R}$, whose gradient map $\nabla u : \Omega \to \Omega^*$ is the unique optimal transport map, furthermore, it satisfies the Monge-Ampère equation:

$$\det D^2 u(x) = \frac{f(x)}{g \circ \nabla u(x)},$$

where $d\mu(x) = f(x)dx$, $d\nu(y) = g(y)dy$, are density functions.

The Brenier theorem has been generalized to the discrete setting in [19]. In the discrete setup, the target domain consists of a finite set of distinct points $\Omega^* = \{p_1, p_2, \ldots, p_n\}$, the target measure is the sum of the Dirac measures, $\nu = \sum_{i=1}^n \nu_i \delta(y - p_i)$, $\sum_{i=1}^n \nu_i = \text{Area}(\Omega)$. For each target point p_i, a supporting plane is constructed as $y = \langle x, p_i \rangle + h_i$, the Brenier potential is the upper envelope of the supporting planes: $u(x) := \max_{i=1}^n \{\langle x, p_i \rangle + h_i\}$. The projection of the Brenier potential is a power Voronoi cell decomposition,

$$\Omega = \bigcup_{i=1}^n W_i(\mathbf{h}), \quad W_i := \{x \in \Omega | \langle x, p_i \rangle + h_i \geq \langle x, p_j \rangle + h_j, \forall j\} \quad (6)$$

Let the area of $W_i(\mathbf{h})$ is $w_i(\mathbf{h})$. We define the convex energy

$$F(\mathbf{h}) = \Sigma_{i=1}^n \nu_i h_i - \int^{\mathbf{h}} \Sigma_{i=1}^n w_i(\eta) d\eta_i,$$

The gradient of the energy is $\nabla F(\mathbf{h}) = (\nu_i - w_i(\mathbf{h}))$ and the Hessian is

$$\frac{\partial^2 F(\mathbf{h})}{\partial h_i \partial h_j} = -\frac{\partial w_i(\mathbf{h})}{\partial h_j} = \begin{cases} \gamma_{ij} & i \neq j \\ -\sum_k \gamma_{ik} & i = j \end{cases}$$

where γ_{ij} is the edge weight, defined as the following: the power Voronoi diagram is dual to a power Delaunay triangulation, edge $e_{ij}(\mathbf{h})$ is dual to edge $\bar{e}_{ij}$:

$$\gamma_{ij}(\mathbf{h}) := \frac{|e_{ij}(\mathbf{h})|}{|\bar{e}_{ij}|} = \frac{|e_{ij}(\mathbf{h})|}{|p_j - p_i|}.$$

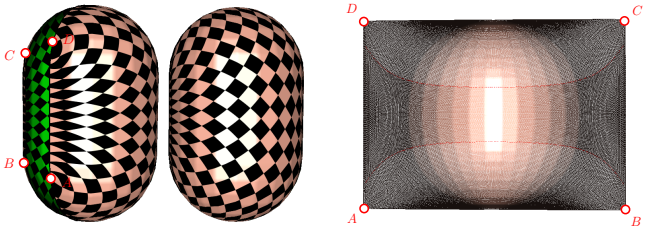

Figure 9: The composition of the conformal and the OT mapping is area-preserving. All checkers have the same size.

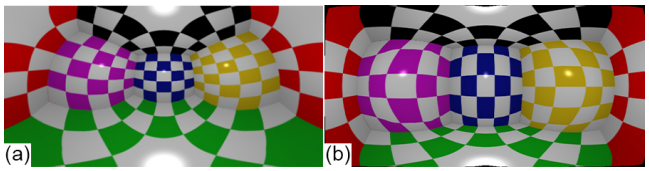

Figure 10: Mapping a cubemap to the Silo surface using (a) conformal mapping and (b) our conformal and OT composition.

The energy is concave [19] and can be optimized using Newton's method to obtain the unique maximal point $\mathbf{h}^*$. The OT map is given by the gradient of the Brenier potential $\nabla u : w_i(\mathbf{h}^*) \to p_i$.

The conformal map φ maps S to a rectangle Ω^*. The target measure ν is constructed as $\nu = \sum_i \nu_i \delta_{\varphi(v_i)}$, where

$$\nu_i = \frac{1}{3} \sum_{f_{ijk} \in F(\mathscr{T})} \text{Area}(f_{ijk}).$$

The source measure is the conventional Lesbesgue measure on the same rectangle $(\Omega, \mathscr{L})$. The OT map is $T : (\Omega, \mathscr{L}) \to (\Omega^*, \nu)$. The composition of conformal and OT $T^{-1} \circ \varphi$ is an area-preserving map from the surface to the rectangle, as in Fig. 9. Observing the checker-board texture mapping, we can see that the mapping is area-preserving, albeit with angle distortions near the boundary.

Fig. 10 shows the environment map to project a 360° view of a cubemap, as in the hypothetical enclosed Silo In Fig. 11, using conformal only and our approach of the area-preserving map achieved by the compsition of the conformal map with the inverse OT map. Additionally, we demonstrate the results of our mapping for two biomedical applications, VC, shown in Fig. 11 (a), an structural bioinformatics, shown in Fig. 11 (b). The insets in both figures highlight in green the amount of information recovered on the Silo surface, which would otherwise be due to the lack of screens on the floor and ceiling. Given the characteristic of the mapping, which only preserves shape features locally, the resultant rendering is visually compelling for non-planar structures. As can be observed in the environment map, Fig. 10, although local angles are preserved, globally, the straight lines of the checkerboard pattern are curved. However, the utility of the mapping can be appreciated, particularly in VC, where a polyp could potentially be positioned in the area of the Silo with missing screens. However, in visualizing the scene using the mapping, the polyp will be visible on the Silo surface, as demonstrated in Fig. 12.

7 User Study

We conducted a user study to compare the effectiveness of three immersive environments – flat-mono (19×11 ft powerwall, referred as **Flat**), curved-mono (Silo in mono, referred as **Curve**), and curved-stereo (Silo in stereo, referred as **Silo**) – for tasks involving 3D datasets. Specifically, our study analyzes qualitative and quantitative metrics that determine how these environments influence user performance, experience, and interaction during tasks related to depth perception, object finding, and pathfinding.

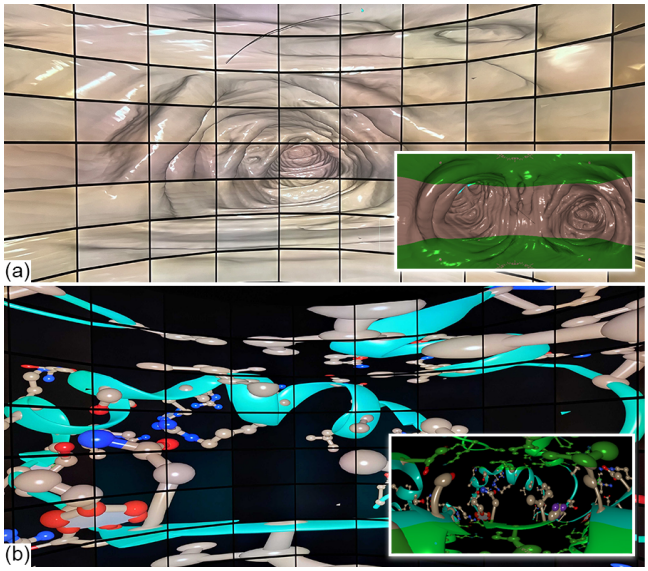

Figure 11: Mapping results in the Silo for (a) VC and (b) protein-folding structure. Insets show the full texture and the missing information recovered by the mapping highlighted in green.

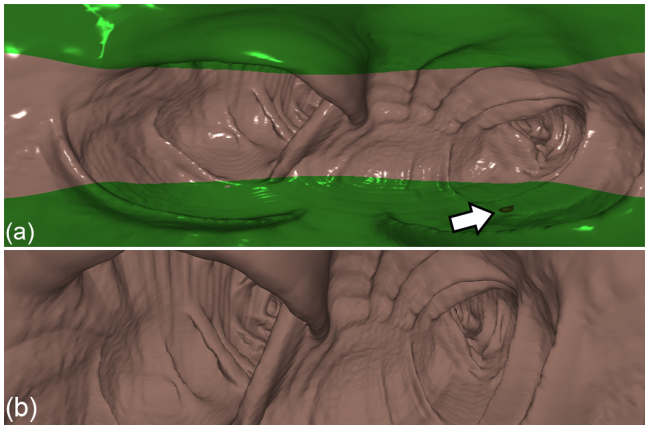

Figure 12: Our mapping reveals a polyp in virtual colonoscopy which was otherwise hidden in the *floor* of the Silo. (a) VC scene mapped on the Silo using our conformal+OT method. The green region highlights recovered information. (b) VC scene without mapping.

7.1 Study Design

Our user study consisted of four tasks, listed below. For each task, the users were asked to complete the task as efficiently and accurately as possible.

T1 was intended to help the participants familiarize themselves with the immersive environment. The scene included a rendering of a town scene with some sign boards. The users were asked to look around and read the signboards. Since this task was for warm-up purposes, the results of this task were not included in the final analysis.

T2 Depth perception using information visualization (Fig. 13(a)). In this task, we presented the users with a 3D scatter plot of the Iris dataset. The participants were asked to compare a pair of points and were asked, *"Which of the two points are closer to you?"* The participants were requested to clearly identify the closer point by replying *"left one"*, *"right one"*, or*"they are equal"*.

T3 Pathfinding and Navigation (Fig. 13(b)). The participants were placed at a starting position in a 3D city scene. Using a controller, the users were asked to navigate the scene by spotting triangular-looking flags in their path and following the direction indicated by the flag. This task was performed three times using three different routes of varying complexity (number of turns, placement of flags, and length of path). All three subtasks were performed in all the environments.

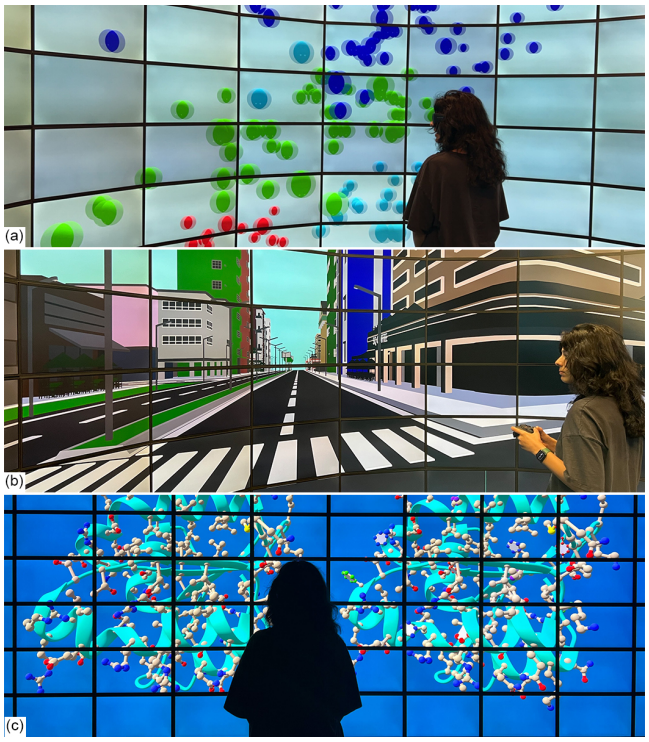

Figure 13: User Study Tasks: (a) Depth Perception - A 3D scatter plot to test participants' depth perception. (b) Objects Identification - Protein structures visualization to identify structural anomalies. (c) Pathfinding - A 3D city navigation task with color-coded flags guiding the participants along different routes.

T4 Objects Identification (Fig. 13(c)). The participants were shown two 3D protein structures: before and after mutation. The mutated structure contained anomalies or additional structures. To assess attention to detail in complex 3D scientific data, the users were asked to identify the anomaly structures in the mutated protein.

The study employed a within-subject design, with each participant completing the tasks in **Flat**, **Curve**, and **Silo**. The order of tasks and the environment in which they were performed were randomized to mitigate potential learning effects or biases. The study was conducted in controlled environmental settings.

Data Collection For qualitative analysis, the participants were asked the NASA-TLX questionnaire following each task in each environment. This provided insights into their cognitive load, mental demand, and overall experience. Additionally, at the completion of a session (all tasks in each environment), the participants were asked to provide any feedback about the session. For quantitative analysis, we recorded the time taken to complete each task (Completion Time) and the correctness of the responses (Effectiveness).

7.2 Results and Discussion

Participants We recruited a total of N=19 (7 women and 12 men) participants, aged 18 to 35. Users were not required to

have any expertise in VR or immersive visualiziation. All participants were screened to ensure normal or corrected-to-normal vision, which was essential for tasks involving depth perception and object identification. The participants were given the option to entirely suspend the study if they experienced cybersickness or take a break if preferred. Out of the 19, only one participant decided to suspend the study, whose partial results have not been included in the analysis. Full details of our evaluations can be found in our Supplementary Materials.

Quantitative Metrics We assess user performance in terms of task completion times and success rates. Overall, the user studies concluded that the Silo demonstrated a superior balance between speed and success rates. Despite Curve's slightly faster times in some tasks, Silo excelled in more complex scenarios, achieving a 100% completion rate for **T3** and consistently high success rates across all tasks, highlighting its overall effectiveness in supporting user performance.

To evaluate the statistical significance of the observed variations between the environments, we performed a one-way ANOVA for both completion times and percentages. We calculated eta squared (η^2) to quantify the proportion of variance in performance attributable to the environment type, highlighting the overall strength of the effects observed. For instances where the ANOVA indicated significant differences, we employed Tukey's HSD post-hoc test to identify specific pairwise differences. To further understand the extent of performance disparities between the facilities, we calculated Cohen's d for these pairwise comparisons, measuring the practical significance of the discrepancies.

Completion Time: For **T2**, Curve and Flat present lower average completion time, 25.28s and 27.89s respectively, compared to Silo, 28.78s. For **T3**, we see a more substantial variation in completion times across the environments. The Silo had the shortest average completion time of 111.86 s, followed by Curve, 120.43s, and Flat delivering the poorest performance with 297.5s. **T4** showed a lower completion time for Curve, 105.08s, followed by Silo 137.88s, and then Flat 160.78s.

Effectiveness: For **T2**, Silo showed a higher success rate of 88.89%, while Curve exhibited a moderate completion percentage of 62.96%, followed by Flat with only 50.00% of participants completing the task. For **T3**, both Silo and Curve achieved a perfect *100%* success rate, whereas Flat fell short with a completion rate of *83.33%*. Meanwhile, for **T4**, Silo again displayed high effectiveness, achieving a completion rate of *88.20%*. Curve followed with a success rate of *79.17%* and Flat lagged with *77.55%*. These results indicate that while Curve provides a balanced environment conducive to task completion, the stereoscopic Silo environment remains the most effective across all tasks.

ANOVA: Statistical analysis revealed a significant difference in completion percentages across facilities for all tasks. For **T2**, ANOVA showed that 31% of the variance in completion percentages was explained by the facility choice ($F(2, 51) = 11.46$, $p = 7.78e\text{-}05$, $\eta^2 = 0.31$). Tukey's HSD test indicates that Silo outperformed both Curve (mean difference = 25.93, p = 0.0079) and Flat (mean difference = 38.89, p = 0.0001). Cohen's d values shows large effect sizes for Flat vs. Silo (d = 1.67) and Curve vs. Silo (d = 1.14), indicating strong practical significance. For **T3**, 17% of the variance was attributed to the facility ($F(2, 51) = 5.59$, $p = 0.0064$, $\eta^2 = 0.17$). Tukey's HSD test found significant differences between both Curve and Flat (mean difference = -16.67, p = 0.0187) and Flat and Silo (mean difference = 16.67, p = 0.0187). Large effect sizes were observed for Flat vs. Curve (d = 0.77) and Flat vs. Silo (d = -0.82), reinforcing a substantial practical difference. For **T4**, ANOVA explained 14% of the variance in completion percentages ($F(2, 51) = 4.14$, $p = 0.0216$, $\eta^2 = 0.14$). Tukey's HSD test found that Silo had a significantly higher completion percentage than Flat (mean difference = 10.65, p = 0.027). Large effect sizes were noted for Flat vs. Silo (d = 0.85) and Curve vs. Silo (d = 0.93), suggesting strong practical significance. Overall, the results emphasize that the Silo facility generally outperforms both Curve and Flat in terms of task completion, with varying degrees of significance and effect sizes across tasks.

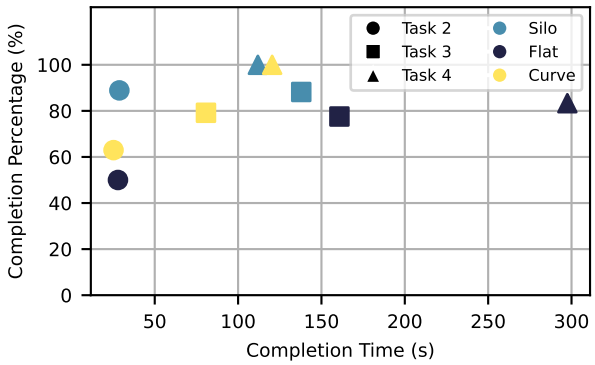

Figure 14: Efficiency of task completion across facilities. Relationship between completion time and completion percentage across evaluated facilities: Silo, Flat, and Curve. Each marker's shape corresponds to a specific task: circles (Task 2 - Depth Perception), squares (Task 3 - Object Identification), and triangles (Task 4 -Pathfinding). The colors represent different facilities: light blue (Silo), dark blue (Flat), and yellow (Curve).

Discussion. A comparison of task completion times with completion percentages (Fig. 14) provides further insights into the performance dynamics of each facility. For **T2**, although Curve recorded the shortest completion time, it did not achieve the highest completion rate, which was attained by Silo at 88.89%, albeit with a slightly longer completion time. Likewise, in **T4**, Curve had a shorter average time compared to Silo; however, Silo surpassed Curve in completion success. We believe one reason for this longer completion time can be attributed to the fact that the stereoscopic environment provided better perception to the participants and, as a result, participants spent more time analyzing the data presented to them. This is reflected in the higher success percentage. Furthermore, for Flat, we noticed that the longer time was mainly due to the participants having to exert physical effort walking across the facility. The most significant disparity was observed in **T3**, where participants managed to successfully complete the task and in the fastest time in the Silo, whereas Flat required substantially more time and yielded a lower completion percentage. This was obvious since the participants spent time rotating the scene using the controller in Flat to be able to see the surroundings, whereas in Silo and Curve, the participants could just turn their head around. Moreover, the flags were better visible in stereoscopic view. Overall, this comparison highlights that while Curve often provides faster task completion, Silo offers a more optimal balance between efficiency and task success, positioning it as the most effective facility for supporting user performance.

7.3 Qualitative Metrics

The NASA Task Load Index (NASA-TLX) (Fig. 15) was used to gather qualitative data, assessing the perceived workload and user experience across six dimensions: Mental Demand, Physical Demand, Temporal Demand, Performance, Effort, and Frustration. To analyze significance, we categorize them into four types: low workload (0-100), moderate workload (100-200), high workload (200-300), and very high workload (300-500).

The analysis using ANOVA results aligns with these visual observations, showing significant differences across most dimensions,

except for frustration ($F(2, 51) = 0.75$, $p = 0.5127$, $\eta^2 = 0.16$). Tukey HSD tests further highlight the Silo's distinctions in specific dimensions. For instance, the mental workload displays a significant difference between Silo and Flat ($F(2, 51) = 6.68$, $p = 0.0297$, $\eta^2 = 0.31$), where Silo scores tend to cluster around lower values, indicating reduced cognitive demand. Similarly, physical workload results show that Silo differs significantly from Curve ($F(2, 51) = 6.14$, $p = 0.0353$, $\eta^2 = 0.14$), with scores suggesting more consistent and lower physical demand. The temporal demand also reveals a notable difference, with Silo showing significantly lower values compared to Flat ($F(2, 51) = 5.70$, $p = 0.0410$, $\eta^2 = 0.17$). In the effort dimension, the Silo facility scores significantly lower than both Curve ($p = 0.0219$) and Flat ($p = 0.0190$), suggesting a less demanding experience for users. The performance dimension further highlights Silo's advantage, as it shows a significant difference compared to Curve ($F(2, 51) = 10.08$, $p = 0.0121$, $\eta^2 = 0.53$), reflecting more favorable performance perceptions. These visual trends, supported by large effect sizes (Cohen's d), emphasize the Silo's practical benefits in creating a more balanced and less demanding environment for task completion. Overall, these results position Silo as the most effective environment, suggesting it can provide an optimal balance of workload and performance for users. The ANOVA results reveal that the Silo facility demonstrates statistically significant advantages over both Flat and Curve in several key NASA-TLX dimensions, namely mental workload, physical workload, temporal demand, performance, and effort. Tukey HSD tests further support these findings, particularly indicating that Silo facilitates reduced mental and physical effort compared to the other facilities. Additionally, Cohen's d values suggest substantial effect sizes, emphasizing the practical significance of Silo's benefits in these areas. No significant differences were observed in the frustration dimension, implying that participants experienced similar levels of frustration across all facilities.

Participant comments, provided in the feedback questionnaire, further support our findings. For instance, several participants expressed that the Silo enhanced spatial awareness and reduced the effort needed to complete the tasks. Some comments include, "*The Silo was much better for me in remembering the context and orientation*," and, "*I did not feel any physical discomfort or disorientation here, and it felt natural.*" The Silo's ability to enhance depth perception was highlighted by one participant who stated, "*This was the only one I could tell the depths of the spheres with any degree of confidence.*" Users also reported feeling more comfortable, with one stating, "*I did not feel any physical discomfort or disorientation here, and it felt natural.*" Object identification was perceived as more effortless, as one participant remarked, "*It was very easy to find all the objects this way.*" Some comments reflected that Silo was the preferred immersive setting, such as, "*Out of the three settings, this was definitely the best one,*" and "*The Silo is definitely my favorite display.*" Naturally, as with any immersive device or facility, three participants left negative feedback about experiencing cybersickness, particularly eye strain, and dizziness.

8 Leasson Learned

Building a large IV facility, such as the Silo, is an expensive and challenging undertaking that entails hardware choices, resource constraints, and technological expertise. A key takeaway from designing and constructing the Silo was the necessity to strike a balance between hardware capabilities and visualization requirements. Naturally, the Silo is only impressive and adequately utilized for data that requires high resolution and panoramic visualization.

While building and designing applications for IV facilities is still an ongoing area of research, such facilities still lack satisfactory support from the OS, graphics driver, and tool availability standpoint. For instance, the internal workings between the NVIDIA driver and the Windows OS desktop manager resulted in each MOSAIC taking as long as 45 minutes to set up. This meant that a node with eight MOSAIC-ed desktops took approximately 6 hours to finish. Consequently, this made testing different MOSAIC configurations unconducive. As mentioned in Sec. 4.2, an important lesson learned for high resolution, high frame-rate, stereo facility is the display cable length between the displays to the GPUs. While we managed to place the nodes as close as possible, with an attempt to minimize noise pollution, it is still not satisfactorily pleasant (visual and noise) and occasionally results in synchronization issues. Regarding available tools, works to support IVs and distributed visualization clusters, such as Equilizer [14] and OmegaLib [15] are not actively maintained, and engines such as Unity3D have suspended active stero support. Thus, having such facilities requires hiring personnel with a strong technical background in graphics pipeline development. As such, we developed our custom OpenGL engine to address complexities relating to GPU affinity, interaction devices, and most importantly, a rendering pipeline that is robust to manage data and visual fidelity for an IV system.

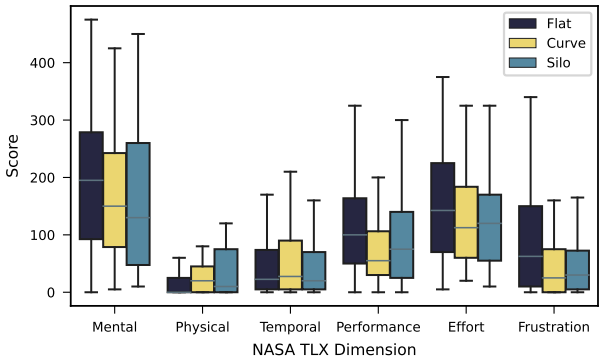

Figure 15: Average NASA-TLX scores across the six dimensions

Based on our experience in building large IV facilities, including the Silo, an essential aspect of lessons learned has always been the maintenance of display hardware. While it is critical to purchase backup monitors, no quantity is sufficient to preserve the longevity of the facility, especially once the displays are out of production. Moreover, with the rise in OLED displays, to the best of our knowledge, no display panels are manufactured that support off-the-shelf active stereo systems as of this date.

For next steps, we plan on researching and developing novel ergonomics and human-computing interaction methods for the stereo cylindrical facility, as well as investigating off-axis stereo rendering for multiple users.

9 Conclusion

In this paper, we presented the design and construction of the Silo, a half-gigapixel immersive stereo facility. Through user studies, we have shown that the cylindrical stereo environment emerges as the most effective environment for immersive and demanding tasks, offering a superior balance between speed, accuracy, and user workload compared to flat and mono settings. Moreover, due to missing displays in the ceiling and floor of the facility, we have developed a novel method that couples conformal and optimal transportation mapping to generate views that capture the entirety of the scene 360° view information onto the Silo screen surface. We also demonstrated the utility of the Silo by exhibiting several applications that enhance user performance and visual exploration in the immersive stereo facility. Finally, we also share and discuss key lessons learned in constructing next-generation large, high-resolution, IV facilities.

REFERENCES

[1] S. Alizadehsalehi and I. Yitmen. Digital twin-based progress monitoring management model through reality capture to extended reality technologies. *Smart and Sustainable Built Environment*, 12(1):200–236, 2023. 4

[2] C. Andrews, A. Endert, B. Yost, and C. North. Information visualization on large, high-resolution displays: Issues, challenges, and opportunities. *Information Visualization*, 10(4):341–355, 2011. 2

[3] ASUS ROG SWIFT. https://rog.asus.com/us/monitors/27-to-31-5-inches/rog-swift-pg278qr-model/spec/. Accessed: July 2024. 3

[4] R. Ball, C. North, and D. A. Bowman. Move to improve: promoting physical navigation to increase user performance with large displays. *ACM SIGCHI Conference on Human Factors in Computing Systems*, pp. 191–200, 2007. 2

[5] A. Batch, A. Cunningham, M. Cordeil, N. Elmqvist, T. Dwyer, B. H. Thomas, and K. Marriott. There is no spoon: Evaluating performance, space use, and presence with expert domain users in immersive analytics. *IEEE Transactions on Visualization and Computer Graphics*, 26(1):536–546, 2019. 2

[6] I. Belkacem, C. Tominski, N. Médoc, S. Knudsen, R. Dachselt, and M. Ghoniem. Interactive visualization on large high-resolution displays: A survey. *Computer Graphics Forum*, p. e15001, 2022. 2

[7] S. Boorboor, Y. Kim, P. Hu, J. M. Moses, B. A. Colle, and A. E. Kaufman. Submerse: Visualizing storm surge flooding simulations in immersive display ecologies. *IEEE Transactions on Visualization and Computer Graphics*, 30(9):6365–6377, 2024. 5

[8] X. Brioso, C. Calderon-Hernandez, J. Irizarry, and D. Paes. Using immersive virtual reality to improve choosing by advantages system for the selection of fall protection measures. *American Society of Civil Engineers*, pp. 146–153, 2019. 3

[9] M. Cavallo, M. Dholakia, M. Havlena, K. Ocheltree, and M. Podlaseck. Dataspace: A reconfigurable hybrid reality environment for collaborative information analysis. *IEEE conference on Virtual Reality and 3D User Interfaces*, pp. 145–153, 2019. 2

[10] C. Cruz-Neira, D. J. Sandin, T. A. DeFanti, R. V. Kenyon, and J. C. Hart. The CAVE: Audio visual experience automatic virtual environment. *Communications of the ACM*, 35(6):64–73, 1992. 1

[11] T. DeFanti, D. Acevedo, R. Ainsworth, M. Brown, S. Cutchin, G. Dawe, K.-U. Doerr, A. Johnson, C. Knox, R. Kooima, et al. The future of the CAVE. *Central European Journal of Engineering*, 1(1):16–37, 2011. 2, 3

[12] T. DeFanti, D. Acevedo, R. Ainsworth, M. Brown, S. Cutchin, G. Dawe, K.-U. Doerr, A. Johnson, C. Knox, R. Kooima, F. Kuester, J. Leigh, L. Long, P. Otto, V. Petrovic, K. Ponto, A. Prudhomme, R. Rao, L. Renambot, D. Sandin, J. Schulze, L. Smarr, M. Srinivasan, P. Weber, and G. Wickham. The future of the CAVE. *Open Engineering*, pp. 16–37, 2011. 1

[13] T. A. DeFanti, G. Dawe, D. J. Sandin, J. P. Schulze, P. Otto, J. Girado, F. Kuester, L. Smarr, and R. Rao. The StarCAVE, a third-generation cave and virtual reality OptIPortal. *Future Generation Computer Systems*, 25(2):169–178, 2009. 2

[14] S. Eilemann, M. Makhinya, and R. Pajarola. Equalizer: A scalable parallel rendering framework. *IEEE Transactions on Visualization and Computer Graphics*, 15(3):436–452, 2009. 4, 9

[15] A. Febretti, A. Nishimoto, V. Mateevitsi, L. Renambot, A. Johnson, and J. Leigh. Omegalib: A multi-view application framework for hybrid reality display environments. *IEEE Virtual Reality*, pp. 9–14, 2014. 9

[16] A. Febretti, A. Nishimoto, T. Thigpen, J. Talandis, L. Long, J. Pirtle, T. Peterka, A. Verlo, M. Brown, D. Plepys, et al. Cave2: a hybrid reality environment for immersive simulation and information analysis. *The Engineering Reality of Virtual Reality, SPIE*, 8649:9–20, 2013. 2, 3

[17] X. Gu, R. Guo, F. Luo, J. Sun, and T. Wu. A discrete uniformization theorem for polyhedral surfaces i. *Journal of Differential Geometry (JDG)*, 109(3):431–466, 2018. 5

[18] X. Gu, F. Luo, J. Sun, and T. Wu. A discrete uniformization theorem for polyhedral surfaces i. *Journal of Differential Geometry (JDG)*, 109(2):223–256, 2018. 5

[19] X. Gu, F. Luo, J. Sun, and S.-T. Yau. Variational principles for minkowski type problems, discrete optimal transport, and discrete monge-ampere equations. *arXiv preprint arXiv:1302.5472*, 2013. 6

[20] X. Gu and S.-T. Yau. *Computational Conformal Geometry*, vol. 3 of *Advanced Lectures in Mathematics*. International Press and Higher Education Press, 2007. 5

[21] R. Hamilton. The Ricci Flow on Surfaces. *A.M.S. Contemp. Math.*, 71(1):237–261, 1986. 5

[22] T. Höllerer, J. Kuchera-Morin, and X. Amatriain. The allosphere: a large-scale immersive surround-view instrument. *Emerging displays technologies: the future of displays and interacton*, pp. 3–es, 2007. 2

[23] M. R. Jakobsen and K. Hornbæk. Is moving improving? some effects of locomotion in wall-display interaction. In *ACM SIGCHI Conference on Human Factors in Computing Systems*, pp. 4169–4178, 2015. 2

[24] T. W. Kuhlen and B. Hentschel. Quo vadis cave: does immersive visualization still matter? *IEEE Computer Graphics and Applications*, 34(5):14–21, 2014. 2

[25] B. Laha, K. Sensharma, J. D. Schiffbauer, and D. A. Bowman. Effects of immersion on visual analysis of volume data. *IEEE Transactions on Visualization and Computer Graphics*, 18(4):597–606, 2012. 1

[26] B. Lee, X. Hu, M. Cordeil, A. Prouzeau, B. Jenny, and T. Dwyer. Shared surfaces and spaces: Collaborative data visualisation in a co-located immersive environment. *IEEE Transactions on Visualization and Computer Graphics*, 27(2):1171–1181, 2020. 2

[27] S. Manjrekar, S. Sandilya, D. Bhosale, S. Kanchi, A. Pitkar, and M. Gondhalekar. Cave: an emerging immersive technology–a review. In *2014 uksim-amss 16th international conference on computer modelling and simulation*, pp. 131–136. IEEE, 2014. 2

[28] J. Marino, W. Zeng, X. Gu, and A. Kaufman. Context preserving maps of tubular structures. *IEEE Transaction on Visualization and Computer Graphics (TVCG)*, 17:1997–2004, 2011. 5

[29] S. Mirhosseini, I. Gutenko, S. Ojal, J. Marino, and A. Kaufman. Immersive virtual colonoscopy. *IEEE Transactions on Visualization and Computer Graphics*, 25(5):2011–2021, 2019. 5

[30] S. Nadeem, Z. Su, W. Zeng, A. Kaufman, and X. Gu. Spherical parameterization balancing angle and area distortions. *IEEE Transaction on Visualization and Computer Graphics (TVCG)*, 23:1663–1676, 2016. 5

[31] D. Paes, J. Irizarry, and D. Pujoni. An evidence of cognitive benefits from immersive design review: Comparing three-dimensional perception and presence between immersive and non-immersive virtual environments. *Automation in Construction*, 130:103849, 2021. 3

[32] C. Papadopoulos, S. Mirhosseini, I. Gutenko, K. Petkov, A. E. Kaufman, and B. Laha. Scalability limits of large immersive high-resolution displays. *IEEE Virtual Reality*, pp. 11–18, 2015. 2, 3

[33] C. Papadopoulos, K. Petkov, A. E. Kaufman, and K. Mueller. The Reality Deck–an immersive gigapixel display. *IEEE Computer Graphics and Applications*, 35(1):33–45, 2015. 1, 2, 3, 4

[34] G. Perelman. The entropy formula for the ricci flow and its geometric applications. *preprint, math.DG/0211159*, 2002. 5

[35] G. Perelman. Finite extinction time for the solutions to the ricci flow on certain threemanifolds. *preprint, math.DG/0307245*, 2003. 5

[36] G. Perelman. Ricci flow with surgery on three-manifolds. *preprint, math.DG/0303109*, 2003. 5

[37] K. Petkov, C. Papadopoulos, M. Zhang, A. E. Kaufman, and X. Gu. Conformal visualization for partially-immersive platforms. In *2011 IEEE Virtual Reality Conference*, pp. 143–150, 2011. doi: 10.1109/VR.2011.5759453 5

[38] K. Petkov, C. Papadopoulos, M. Zhang, A. E. Kaufman, and X. Gu. Interactive visibility retargeting in vr using conformal visualization. *IEEE Transactions on Visualization and Computer Graphics*, 18(7):1027–1040, 2012. 2

[39] K. Ponto, J. Kohlmann, and R. Tredinnick. Dscvr: designing a commodity hybrid virtual reality system. *Virtual Reality*, 19:57–70, 2015. 2

[40] K. Reda, A. Johnson, V. Mateevitsi, C. Offord, and J. Leigh. Scalable visual queries for data exploration on large, high-resolution 3D displays. *IEEE High Performance Computing, Networking Storage and*

Analysis, pp. 196–205, 2012. 2

[41] S. Safikhani, S. Keller, G. Schweiger, and J. Pirker. Immersive virtual reality for extending the potential of building information modeling in architecture, engineering, and construction sector: systematic review. *International Journal of Digital Earth*, 15(1):503–526, 2022. 4

[42] Z. Su, W. Zeng, R. Shi, Y. Wang, J. Sun, and X. Gu. Area preserving brain mapping. In *Proceedings of the IEEE Conference on Computer Vision and Pattern Recognition*, pp. 2235–2242, 2013. 6

[43] W. P. Thurston. *The Geometry and Topology of Three-Manifolds*, vol. 27. American Mathematical Society, 2022. 2

[44] C. Villani. *Topics in Optimal Transportation*, vol. 58. American Mathematical Society, 2003. 2, 6

[45] C. Villani. *Optimal transport: old and new*, vol. 338. Springer Science & Business Media, 2008. 6

[46] Volfoni RF Active 3D System. http://volfoni.com/en/activhub-rf50/. Accessed: July 2024. 4

[47] X. Zhao, K. Mueller, W. Zeng, A. Kaufman, W. Xu, and X. Gu. Conformal magnifier: A fcous + context technique with minimal distortion. *IEEE Transaction on Visualization and Computer Graphics (TVCG)*, 18:1928–1941, 2012. 5, 6

[48] X. Zhao, Z. Su, X. D. Gu, A. Kaufman, J. Sun, J. Gao, and F. Luo. Area-preservation mapping using optimal mass transport. *IEEE Transaction on Visualization and Computer Graphics (TVCG)*, 19:2838–2847, 2013. 5, 6